

From QCD-based hard-scattering to nonextensive statistical mechanical descriptions of transverse momentum spectra in high-energy pp and $p\bar{p}$ collisions

Cheuk-Yin Wong,^{1,*} Grzegorz Wilk,^{2,†} Leonardo J. L. Cirto,^{3,‡} and Constantino Tsallis^{3,4,§}

¹*Physics Division, Oak Ridge National Laboratory, Oak Ridge, Tennessee 37831, USA*

²*National Centre for Nuclear Research, Warsaw 00-681, Poland*

³*Centro Brasileiro de Pesquisas Físicas & National Institute of Science and Technology for Complex Systems, Rua Xavier Sigaud 150, 22290-180 Rio de Janeiro-RJ, Brazil*

⁴*Santa Fe Institute, 1399 Hyde Park Road, Santa Fe, NM 87501, USA*

Transverse spectra of both jets and hadrons obtained in high-energy pp and $p\bar{p}$ collisions at central rapidity exhibit power-law behavior of $1/p_T^n$ at high p_T . The power index n is 4-5 for jet production and is 6-10 for hadron production. Furthermore, the hadron spectra spanning over 14 orders of magnitude down to the lowest p_T region in pp collisions at LHC can be adequately described by a single nonextensive statistical mechanical distribution that is widely used in other branches of science. This suggests indirectly the possible dominance of the hard-scattering process over essentially the whole p_T region at central rapidity in high energy pp and $p\bar{p}$ collisions. We show here direct evidences of such a dominance of the hard-scattering process by investigating the power indices of UA1 and ATLAS jet spectra over an extended p_T region and the two-particle correlation data of the STAR and PHENIX Collaborations in high-energy pp and $p\bar{p}$ collisions at central rapidity. We then study how the showering of the hard-scattering product partons alters the power index of the hadron spectra and leads to a hadron distribution that may be cast into a single-particle nonextensive statistical mechanical distribution. Because of such a connection, the nonextensive statistical mechanical distribution may be considered as a lowest-order approximation of the hard-scattering of partons followed by the subsequent process of parton showering that turns the jets into hadrons, in high energy pp and $p\bar{p}$ collisions.

PACS numbers: 05.90.+m, 24.10.Pa, 25.75.Ag, 24.60.Ky

I. INTRODUCTION

Transverse momentum distribution of jets and hadrons provide useful information on the collision mechanisms and their subsequent dynamics. The transverse spectra of jets in high-energy pp and $p\bar{p}$ experiments at high p_T and central rapidity exhibit a power-law behavior of $1/p_T^n$ with the power index $n \sim 4 - 5$, which indicates that jets are scattered partons produced in relativistic hard-scattering processes [1–13]. On the other hand, the power index for hadron spectra are in the range of 6 to 10, slightly greater than those for jets [2, 9–13], revealing that hadrons are showering products from jets, and the hadron spectra are modified from the jet spectra but retaining the basic power-law structure of the jet spectra. It was found [11–15] recently that the hadron spectra spanning over 14 decades of magnitude from the lowest to the highest p_T at central rapidity can be adequately described by a single nonextensive statistical mechanical distribution that is widely used in other branches of sciences [16, 17],

$$F(p_T) = A \left[1 - (1 - q) \frac{p_T}{T} \right]^{1/(1-q)}. \quad (1)$$

Such a distribution with $q = 1 + 1/n$ is phenomenologically equivalent to the quasi-power law interpolating formula introduced by Hagedorn [18] and others [19]

$$F(p_T) = A \left(1 + \frac{p_T}{p_0} \right)^{-n}, \quad (2)$$

for relativistic hard scattering. Both Eqs. (1) and (2) have been widely used in the phenomenological analysis of multiparticle productions, cf., for example, [20–28] and references therein.

It is of interest to know why such a nonextensive statistical mechanical distribution (1) may be a useful concept for hadron production. It may also be useful to contemplate its possible implications. The shape of the spectrum reflects the complexity, or conversely the simplicity, of the underlying production mechanisms. If there are additional significant contributions from other mechanisms, the specification of the spectrum will require degrees of freedom additional to those of the relativistic hard-scattering model. The small number of apparent degrees of freedom of the spectrum over such a large p_T region¹ suggests the possible dominance of the hard-scattering process over essentially the whole region of p_T at central rapidity [11–14].

* wongc@ornl.gov
 † wilk@fuw.edu.pl
 ‡ cirto@cbpf.br
 § tsallis@cbpf.br

¹ There are only three degrees of freedom in Eq. (1): A , q (or equivalently n), and T . Notice that three degrees of freedom are almost the minimum number to specify a spectrum. Our spectrum is therefore very simple. It is interesting therefore that the counting of the degrees of freedom in our case can lead to the

The counting of the degrees of freedom provides merely an indirect evidence for the dominance of the hard-scattering process over the whole p_T region. We would like to search for direct evidences for such a dominance in three different ways. The hard scattering process is characterized by the production of jets whose transverse spectra carries the signature of the power index of $n \sim 4 - 5$ at central rapidity [12–14]. The relevant data come from well-defined jets with transverse momenta greater than many tens of GeV obtained in D0, ALICE, and CMS Collaborations [29–31]. To seek direct supporting evidences of jet production by the hard-scattering process over the lower- p_T region, we examine the experimental UA1 and ATLAS data which give the invariant cross sections for the production of jets from the low- p_T region (of a few GeV) to the high- p_T region (up to 150 GeV) [32, 33]. If the power index n of the UA1 and ATLAS jet spectra at central rapidity is close to 4 - 5, it will constitute a direct evidence of the dominance of the hard-scattering process over the extended p_T region, for $p\bar{p}$ and pp collisions at high energies. In such an analysis, we need to take into account important p_T -dependencies of the structure function and the running coupling constant by refining the analytical formula of the hard-scattering integral.

The hard-scattering process is characterized by the production of jets as angular clusters of hadrons. We can seek additional direct evidences for the dominance of the hard-scattering process by searching for hadron angular clusters on the near-side using the two-particle correlation data in high-energy pp collisions from STAR and PHENIX Collaborations [34–43]. Two-particle angular correlation data are specified by the azimuthal angular difference $\Delta\phi$ and the pseudorapidity difference $\Delta\eta$ of the two particles. If hadrons associated with a low- and high- p_T trigger are correlated at $(\Delta\phi, \Delta\eta) \sim 0$ on the near-side, it will constitute an indication of the dominance of the hard-scattering process over essentially the whole p_T region.

Finally, the hard-scattering process is characterized by the production of two jets of particles. We can seek an additional direct evidence for the other partner jet by searching for angular clusters of associated hadrons on the away-side in two-particle correlation data from STAR and PHENIX Collaborations [34–43]. A ridge of hadrons on the away-side at $\Delta\phi \sim \pi$ associated with a low- p_T and high- p_T trigger will indicate the production of the partner jet by the hard-scattering process over the whole p_T region.

While our search has been stimulated by the simplicity of the hadron p_T spectrum, it should be mentioned that the importance of the production of jets with p_T of a few GeV (minijets) has already been well emphasized in the earlier work of [7], and the production of the low- p_T

jet (minijets) in the low- p_T region has been pointed in the work of [38–41]. We are seeking here a synthesizing description linking these advances together into a single and simplifying observation on the dominance of the hard-scattering over the whole p_T region, with a special emphasis on the production mechanism. Such a complementary and synthesizing viewpoint may serve the useful purposes of helping guide our intuition and summarizing important features of the collision process.

After examining the experimental evidences for the dominance of the relativistic hard-scattering process in the whole p_T region, we would like to understand how jets turn into hadrons and in what way the jet spectra evolves to become the hadron spectra by parton showering. Our understanding may allow us to bridge the connection between the hard-scattering process for jet production and its approximate representation by a nonextensive statistical mechanical distribution for hadron production. In consequence, the dominance of the hard-scattering process over the whole p_T region may allow the nonextensive statistical mechanical distribution to describe the observed hadron transverse spectra spanning the whole p_T region at central rapidity, in pp collisions at LHC.

In this paper, we restrict our attention to the central rapidity region at $\eta \sim 0$ and organize the paper as follows. In Section II, we review and refine the analytical results for the relativistic hard-scattering process. We use the analytical results to analyze the spectra for high- p_T jets in Section III. We note that jet spectra carry the signature of the hard-scattering process with a power index $n \sim 4 - 5$ at central rapidity. In Section IV, we study the UA1 and ATLAS data which extend from the low- p_T region of a few GeV to the high- p_T region up to 150 GeV. We find that the power index for jet production is approximately 4 - 5, supporting the dominance of the hard-scattering process over the extended p_T region at central rapidity. In Section V, we seek additional evidences of the hard-scattering process from two-particle correlation data. In Section VI, we study the effects of parton showering on the evolution of the jet spectra to the hadron spectra. In Section VII, we examine the regularization and further approximation of the relativistic hard-scattering integral to bring it to the form of the nonextensive statistical mechanics. In Section VIII, we analyze hadron spectra using the nonextensive statistical mechanical distribution. We present our concluding summary and discussions in Section IX.

II. APPROXIMATE HARD-SCATTERING INTEGRAL

We would like to review and summarize the results of the hard-scattering integral obtained in our earlier works in [8, 12–14, 44] so that we can refine previous analytical results. We consider the collision of A and B in the center-of-mass frame at an energy \sqrt{s} with the detected particle c coming out at $\eta \sim 0$ in the reaction $A + B \rightarrow c + X$ as a result of the relativistic hard-

suggestion of possible hard-scattering dominance and the successful search for supporting direct evidences as we describe in the present work.

scattering of partons a from A with parton b from B . Upon neglecting the intrinsic transverse momentum and rest masses, the differential cross section in the lowest-order parton-parton elastic collisions is given by

$$\frac{E_c d^3\sigma(AB \rightarrow cX)}{dc^3} = \sum_{ab} \int dx_a dx_b G_{a/A}(x_a) G_{b/B}(x_b) \times \frac{E_c d^3\sigma(ab \rightarrow cX')}{dc^3}, \quad (3)$$

where we use the notations in Ref. [12] with c the momentum of the produced parton, x_a and x_b the forward light-cone variables of colliding partons a and b in A and B , respectively and $d\sigma(ab \rightarrow cX')/dt$ the parton-parton invariant cross section.

We are interested in the production of particle c at $\theta_{CM} = 90^\circ$ for which analytical approximate results can be obtained. We integrate over dx_a in Eq. (3) by using the delta-function constraint in the parton-parton invariant cross section, and we integrate over dx_b by the saddle-point method to write

$$[x_{a0} G_{a/A}(x_a)][x_{b0} G_{b/B}(x_b)] = e^{f(x_b)}. \quad (4)$$

We expand $f(x_b)$ about its minimum at x_{b0} . We obtain

$$\int dx_b e^{f(x_b)} g(x_b) \sim e^{f(x_{b0})} g(x_{b0}) \sqrt{\frac{2\pi}{-\partial^2 f(x_b)/\partial x_b^2|_{x_b=x_{b0}}}}.$$

For simplicity, we assume $G_{a/A}$ and $G_{b/B}$ to have the same form. At $\theta_c \sim 90^\circ$ in the CM system, the minimum value of $f(x_b)$ is located at

$$x_{b0} = x_{a0} = 2x_c, \quad \text{and} \quad x_c = \frac{c_T}{\sqrt{s}}. \quad (5)$$

We get

$$E_C \frac{d^3\sigma(AB \rightarrow cX)}{dc^3} \sim \sum_{ab} B[x_{a0} G_{a/A}(x_{a0})][x_{b0} G_{b/B}(x_{b0})] \times \frac{d\sigma(ab \rightarrow cX')}{dt}, \quad (6)$$

where

$$B = \frac{1}{\pi(x_{b0} - c_T^2/x_{cs})} \sqrt{\frac{2\pi}{-\partial^2 f(x_b)/\partial x_b^2|_{x_b=x_{b0}}}}. \quad (7)$$

For the case of $x_a G_{a/A}(x_a) = A_a(1-x_a)^{g_a}$, we find

$$-\left. \frac{\partial^2 f(x_b)}{\partial x_b^2} \right|_{x_b=x_{b0}} = \frac{2g(1-x_c)}{x_c(1-x_{a0})(1-x_{b0})}, \quad (8)$$

and we obtain²

$$E_C \frac{d^3\sigma(AB \rightarrow cX)}{dc^3} \sim \sum_{ab} A_a A_b \frac{(1-x_{a0})^{g_a + \frac{1}{2}} (1-x_{b0})^{g_b + \frac{1}{2}}}{\sqrt{\pi g_a} \sqrt{x_c(1-x_c)}} \times \frac{d\sigma(ab \rightarrow cX')}{dt}. \quad (9)$$

The above analytical result differs from the previous result of Eq. (9) of Ref. [12], where the factor that appears in the above equation

$$(1-x_{a0})^{\frac{1}{2}} (1-x_{b0})^{\frac{1}{2}} / \sqrt{(1-x_c)} \quad (10)$$

was approximated to be unity. We wish to retain such a factor in order to obtain a more accurate determination of the power index, in cases where c_T may be a substantial fraction of \sqrt{s} .

If the basic process is $gg \rightarrow gg$, the cross section at $\theta_c \sim 90^\circ$ [45] is

$$\frac{d\sigma(gg \rightarrow gg)}{dt} \sim \frac{9\pi\alpha_s^2}{16c_T^4} \left[\frac{3}{2} \right]^3. \quad (11)$$

If the basic process is $qq' \rightarrow qq'$, the cross section at $\theta_c \sim 90^\circ$ [45] is

$$\frac{d\sigma(qq' \rightarrow qq')}{dt} = \frac{4\pi\alpha_s^2}{9c_T^4} \frac{5}{16}. \quad (12)$$

If the basic process is $gq \rightarrow gq'$, the cross section at $\theta_c \sim 90^\circ$ [45] is

$$\frac{d\sigma(gq \rightarrow gq')}{dt} = \frac{5\pi\alpha_s^2}{4c_T^4} \frac{11}{36}. \quad (13)$$

In all cases, the differential cross section varies as $d\sigma(ab \rightarrow cX')/dt \sim \alpha_s^2/(c_T^2)^2$.

III. THE POWER INDEX IN JET PRODUCTION AT HIGH p_T

Our earlier investigation on the effects of multiple collisions indicates that without a centrality selection in minimum-biased events, the differential cross section for the production of partons at high- p_T will be dominated by the contribution from a single parton-parton scattering that behaves as $1/c_T^4$ [12, 46–49]. It suffices to consider only the results of the single parton-parton collision as given in Eq. (9) which can be compared directly with the transverse differential cross sections for hadron jet and isolated photon production.

From the results in the parton-parton cross sections in Eqs. (11,12,13), the approximate analytical formula for hard-scattering invariant cross section σ_{inv} , for $A+B \rightarrow c+X$ at $\eta \sim 0$, is

$$E_c \frac{d^3\sigma(AB \rightarrow cX)}{dc^3} \Big|_{\eta \sim 0} \propto \frac{\alpha_s^2 (1-x_{a0}(c_T))^{g_a + \frac{1}{2}} (1-x_{b0}(c_T))^{g_b + \frac{1}{2}}}{c_T^4 \sqrt{c_T/\sqrt{s}} \sqrt{1-x_c(c_T)}}. \quad (14)$$

We analyze the c_T spectra by using a running coupling constant

$$\alpha_s(Q(c_T)) = \frac{12\pi}{27 \ln(C + Q^2/\Lambda_{\text{QCD}}^2)}, \quad (15)$$

² In Eq. (23) of the earlier work of [12], there was a typographical error in the quantity x_{b0} in the denominator under the square root sign, which should be x_c .

where Λ_{QCD} is chosen to be 0.25 GeV to give $\alpha_s(M_Z^2) = 0.1184$ [50], and the constant C is chosen to be 10, both to give $\alpha_s(Q \sim \Lambda_{\text{QCD}}) \sim 0.6$ in hadron spectroscopy studies [51] and to regularize the coupling constant for small values of $Q(c_T)$. We identify Q as c_T and search for n by writing the invariant cross section for jet production as

$$\sigma_{\text{inv}} \equiv E_c \left. \frac{d^3\sigma(AB \rightarrow cX)}{dc^3} \right|_{\eta \sim 0} = \frac{A\alpha_s^2(Q^2(c_T))(1-x_{a0}(c_T))^{g_a+\frac{1}{2}}(1-x_{b0}(c_T))^{g_b+\frac{1}{2}}}{c_T^n \sqrt{1-x_c(c_T)}}, \quad (16)$$

where the power index n for perturbative QCD has the value of 4.5.

We identify the parton c with the produced jet and we define the jet transverse rapidity y_T as the logarithm of c_T/\sqrt{s} ,

$$y_T = \ln \left(\frac{c_T}{\sqrt{s}} \right), \quad e^{y_T} = \frac{c_T}{\sqrt{s}}, \quad (17)$$

then the results in Eq. (16) gives

$$\frac{\partial \ln \sigma_{\text{inv}}}{dy_T} = \frac{\partial \alpha_s}{dy_T} - \frac{2(g_a + g_b + 1)e^{y_T}}{1 - 2e^{y_T}} - n + \frac{e^{y_T}}{2(1 - e^{y_T})} \quad (18)$$

and

$$\frac{\partial^2 \ln \sigma_{\text{inv}}}{dy_T^2} = \frac{\partial^2 \alpha_s}{dy_T^2} - \frac{2(g_a + g_b + 1)e^{y_T}}{(1 - 2e^{y_T})^2} + \frac{e^{y_T}}{2(1 - e^{y_T})^2}. \quad (19)$$

Therefore in the $(\ln \sigma_{\text{inv}}) - (\ln E_T(c_T))$ plot in Fig. 1, the slope $(\partial \ln \sigma_{\text{inv}}/dy_T)$ at small values of E_T gives approximately the power index n and the second derivative of $\ln \sigma_{\text{inv}}$ with respect to $\ln E_T$ at large values of E_T gives approximately the power index $g_a + g_b$ of the structure function. The exponential index $g_a = g_b$ for the structure function of a gluon varies from 6 to 10 in different structure functions [5, 52]. We shall take $g_a = 6$ from [5].

With our refinement of the hard-scattering integral in Eq. (9), our analytical invariant cross section of Eq. (16) differs from that in our earlier work in [12] in the presence of an extra energy- and p_T -dependent factor of Eq. (10) and a slightly different running coupling constant. We shall re-examine the power indices with Eq. (16). We wish to obtain a more accurate determination of the power indices, in cases where c_T may be a substantial fraction of the collision energy \sqrt{s} . We also wish to use Eq. (16) to calibrate the signature of the power indices for jets at high p_T , where jets can be better isolated, to test in the next section the power indices for jets extending to the lower p_T region, where jets are more numerous and harder to isolate.

Using Eq. (16), we find that the $d\sigma/d\eta E_T dE_T|_{\eta \sim 0}$ data from the D0 Collaboration [29] for hadron jet production within $|\eta| < 0.5$ can be fitted with $n=4.39$ for $\bar{p}p$ collisions at $\sqrt{s}=1.8$ TeV, and with $n=4.47$ for $\bar{p}p$ collisions at $\sqrt{s}=0.630$ TeV, as shown in Fig. 1.

In another comparison with the ALICE data for jet production in pp collisions at $\sqrt{s} = 2.76$ TeV at the LHC

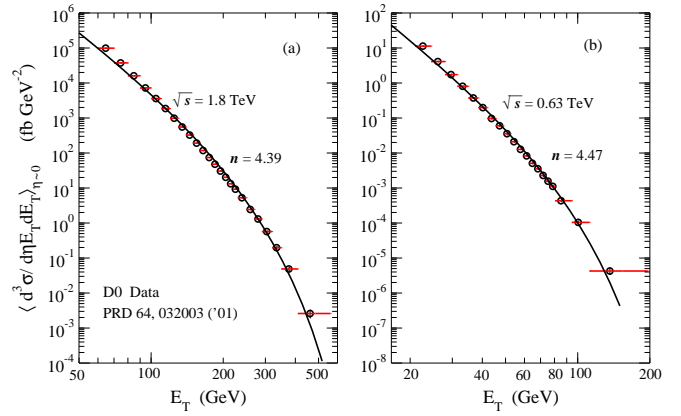


FIG. 1. (Color online) Comparison of the relativistic hard-scattering model results for jet production, Eq. (16) (solid curves), with experimental $d\sigma/d\eta E_T dE_T|_{\eta \sim 0}$ data from the D0 Collaboration [29], for hadron jet production within $|\eta| < 0.5$, in $\bar{p}p$ collision at (a) $\sqrt{s}=1.80$ TeV, and (b) $\sqrt{s}=0.63$ TeV.

within $|\eta| < 0.5$ [30] in Fig. 2, the power index is $n=4.78$ for $R = 0.2$, and is $n=4.98$ for $R = 0.4$ (Table I). In Fig. 3, the power index is $n=5.39$, for CMS jet differential cross section in pp collisions at $\sqrt{s} = 7$ TeV at the LHC within $|\eta| < 0.5$ and $R = 0.5$ [31].

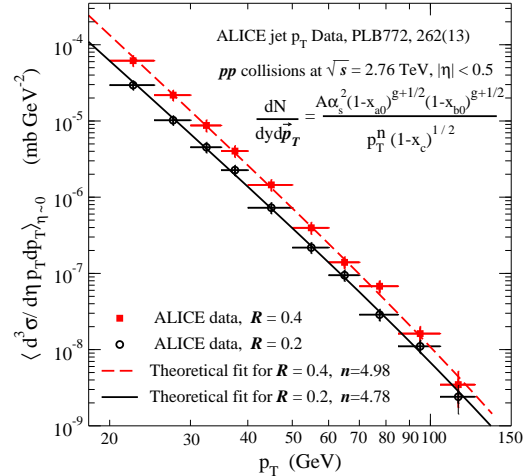


FIG. 2. (Color online) Comparison of the relativistic hard-scattering model results for jet production, Eq. (16) (solid curves), with experimental $d\sigma/d\eta E_T dE_T|_{\eta \sim 0}$ data from the ALICE Collaboration [30], for jet production within $|\eta| < 0.5$, in pp collision at 2.76 TeV for $R=0.4$, and $R=0.2$.

The power indices extracted from the hadron jet spectra in D0 [29], [30], and CMS [31] are listed in Table I. The extracted D0 power indices are smaller than those extracted previously in [12] by 0.2 units, as the highest transverse momenta are substantial fractions of the collision energy. In the other cases, the change of the power indices from our earlier work in [12] are small as their highest transverse momenta are substantially

smaller than the collision energies.

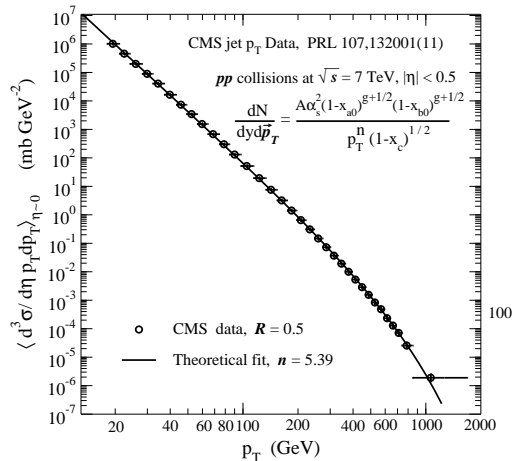


FIG. 3. Comparison of the relativistic hard-scattering model results for jet production, Eq. (16) (solid curves), with experimental $d\sigma/d\eta E_T dE_T|_{\eta\sim 0}$ data from the CMS Collaboration [31], for jet production within $|\eta|<0.5$, in pp collisions at 7 TeV.

With the jet spectra at high p_T from the D0, ALICE and CMS Collaborations, we find that the signature for jet production is a power index in the range of 4.5 to 5.4, with a small variation that depend on \sqrt{s} and R as shown in Table I. While these power indices are close to the lowest-order pQCD prediction of 4.5, there appears to be a consistent tendency for n to increase slightly as \sqrt{s} and R increases. Such an increase may arise from higher-order pQCD effects. We can envisage the physical picture that as the jet evolves by parton showering, the number of generations of parton branching will increase with a greater collision energy \sqrt{s} or a greater opening angle R . A greater \sqrt{s} or a larger R value corresponds to a later stage of the evolution of the parton showering and they will lead naturally to a slightly greater value of the power index n .

TABLE I. The power index n for the jet spectra in $\bar{p}p$ and pp collisions. Here, R is the jet cone angular radius used in the jet search algorithm.

	\sqrt{s}	p_T Region	R	η	n
D0[29]	$\bar{p}p$ 1.80TeV	$64 < p_T < 461 \text{ GeV}$	0.7	$ \eta < 0.7$	4.39
D0[29]	$\bar{p}p$ 0.63TeV	$22 < p_T < 136 \text{ GeV}$	0.7	$ \eta < 0.7$	4.47
ALICE[30]	pp 2.76TeV	$22 < p_T < 115 \text{ GeV}$	0.2	$ \eta < 0.5$	4.78
ALICE[30]	pp 2.76TeV	$22 < p_T < 115 \text{ GeV}$	0.4	$ \eta < 0.5$	4.98
CMS [31]	pp 7TeV	$19 < p_T < 1064 \text{ GeV}$	0.5	$ \eta < 0.5$	5.39

The signature of the power indices for the production of jets at high p_T can be used to identify the nature of the jet production process at low p_T . If the power indices in the production in the lower- p_T region are similar, then the jets in the lower- p_T region and the jets in the high- p_T region have the same spectral shape and can be considered to originate from the same production

mechanism, extending the dominance of the relativistic hard-scattering process to the lower- p_T region.

IV. JET PRODUCTION IN AN EXTENDED REGION FROM LOW TO HIGH p_T

The analysis in the last section was carried out for jets with a transverse momentum greater than 19 GeV. It is of interest to find out whether the perturbative QCD power index remains a useful concept when we include also the production of jet-like energy clusters (mini-jets) at lower transverse momenta. In order to apply the power-law (16) to the whole range of c_T , we need to regularize it by the replacement³,

$$\frac{1}{c_T^2} \rightarrow \frac{1}{1 + m_T^2/m_{T0}^2}. \quad (20)$$

or alternatively as

$$\frac{1}{c_T} \rightarrow \frac{1}{1 + m_T/m_{T0}}. \quad (21)$$

The quantity m_{T0} measures the average transverse mass of the detected jet in the hard-scattering process. Upon choosing the regularization (20), the differential cross section $d^3\sigma(AB \rightarrow pX)/dyd\vec{p}_T$ in (16) is then regularized as

$$\left. \frac{d^3\sigma(AB \rightarrow pX)}{dyd\vec{p}_T} \right|_{y\sim 0} \propto \frac{\alpha_s^2(Q^2(c_T))(1-x_{a0}(c_T))^{g_a+1/2}(1-x_{b0}(c_T))^{g_b+1/2}}{[1 + m_T^2(c_T)/m_{T0}^2]^{n/2} \sqrt{1-x_c(c_T)}}. \quad (22)$$

We fit the inclusive UA1 jet cross sections at $\eta \sim 0$ [32] as a function of the jet p_T for $\bar{p}p$ collisions with the above equation, and we find that $n=4.47$ and $m_{T0}=0.267$ GeV for $\bar{p}p$ collisions at $\sqrt{s}=564$ GeV, and $n=4.73$ and $m_{T0}=0.363$ GeV for $\bar{p}p$ collisions at $\sqrt{s}=630$ GeV.

The ATLAS p_T spectra for pp collisions at 7 TeV also extend to the region of a few GeV. It is of interest to find out what are the power indices for these collisions. We show in Fig. 5 the comparison of the results of Eq. (22) with the ATLAS data at $\eta \sim 0$ [33]. We find that $n=5.03$ for $R = 0.4$ and $n = 5.29$ for $R=0.6$. Because the data start with p_T of a few GeV, the fits and the extracted value of n are insensitive to the variation of the m_{T0}

³ So far, the only rationale behind this is that, in the QCD approach, large c_T partons probe small distances (with small cross sections). With diminishing of c_T , these distances become larger (and cross sections are increasing) and, eventually, they start to be of the order of the nucleon size (actually it happens around $c_T \simeq c_{T0} \sim 1/r_{\text{nucleon}}$ or $m_T \simeq m_{T0}$). At that point the cross section should stop rising, i.e., it should not depend anymore on the further decreasing of transverse momentum c_T . The scale parameter m_{T0} can then be identified with m_{T0} here. Similar idea was employed when proposing Eq. (15).

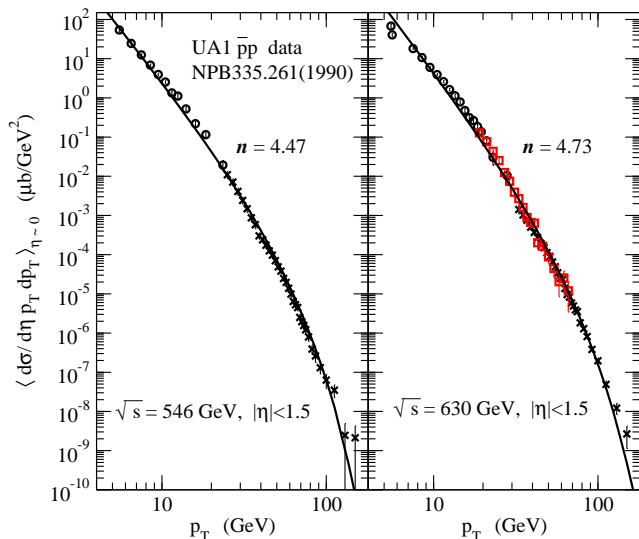


FIG. 4. (Color online) Comparison of the relativistic hard-scattering model results for jet production, Eq. (22) (solid curves), with experimental $d\sigma/d\eta p_T dp_T$ data from the UA1 Collaboration [32], for jet production within $|\eta| < 1.5$, in $\bar{p}p$ collision at (a) $\sqrt{s} = 0.546$ TeV, and (b) $\sqrt{s} = 0.63$ TeV.

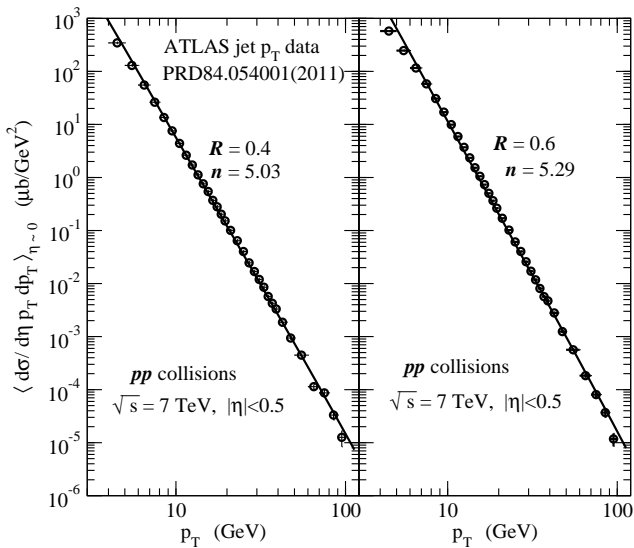


FIG. 5. Comparison of the relativistic hard-scattering model results for jet production, Eq. (22) (solid curves), with experimental $d\sigma/d\eta p_T dp_T|_{|\eta \sim 0}$ data from the ATLAS Collaboration [33], for jet production within $|\eta| < 0.5$, in pp collision at $\sqrt{s} = 7$ TeV, with (a) $R = 0.4$ and (b) $R = 0.6$.

values so that there is an ambiguity in the product of the normalization and m_{T0} in the analysis. The fits in Fig. (5) have been obtained with $m_{T0} = 1$ GeV. The value of n is related to the slope of the curves in Fig. 5.

We list in Table II the power indices extracted from UA1 and ATLAS for the extended p_T region from a few GeV to the high- p_T region. It should be mentioned that the importance of the production of jets with p_T of a

TABLE II. The power index n extracted from jet production in $\bar{p}p$ and pp collisions in the extended p_T region from a few GeV to the high- p_T region.

	\sqrt{s}	p_T Region	R	η	n
UA1[32]	$\bar{p}p$ 0.564 TeV	$5.5 < p_T < 150$ GeV	0.75	$ \eta < 1.5$	4.47
UA1[32]	$\bar{p}p$ 0.63 TeV	$5.5 < p_T < 150$ GeV	0.75	$ \eta < 1.5$	4.73
ATLAS[33]	pp 7 TeV	$4.5 < p_T < 95$ GeV	0.4	$ \eta < 0.5$	5.03
ATLAS[33]	pp 7 TeV	$4.5 < p_T < 95$ GeV	0.6	$ \eta < 0.5$	5.29

few GeV (minijets) has already been emphasized in the earlier work of [7].

By comparing the power indices obtained in Table I for D0, ALICE, and CMS for jets at high p_T with those for UA1 and ATLAS for jets in the lower- p_T region in Table II, we note that these power indices are very similar. The corresponding power index values are nearly the same, and the changes of the power index with respect to \sqrt{s} and R are nearly the same. They can be considered to originate from the same relativistic hard-scattering mechanism, indicating the dominance of the hard-scattering process over the extended p_T region from a few GeV to about 100 GeV.

V. ADDITIONAL EVIDENCES OF JET PRODUCTION FROM TWO-PARTICLE CORRELATION DATA

In addition to the spectral shape, we seek additional evidences of jet production in the low- p_T region from experimental two-particle correlations measurements, which consist of correlations on the near-side and the away-side. We shall first examine near-side correlations.

The experimental distribution of near-side particles associated with a trigger particle of momentum p_T^{trig} in pp collisions can be described well by [42, 43]

$$\frac{dN_{\text{jet}}^{pp}}{p_T dp_T d\Delta\eta d\Delta\phi} = N_{\text{jet}} \frac{\exp\{(m - \sqrt{m^2 + p_T^2})/T_{\text{jet}}\}}{T_{\text{jet}}(m + T_{\text{jet}})} \times \frac{1}{2\pi R^2} e^{-[(\Delta\phi)^2 + (\Delta\eta)^2]/2R^2}, \quad (23)$$

where by assumption of hadron-parton duality m can be taken as the pion mass m_π , N_{jet} is the total number of near-side (charged) associated particles in a pp collision, and T_{jet} is the jet inverse slope (“temperature”) parameter of the “ pp jet component”. We find that the parameters N_{jet} and T_{jet} vary linearly with p_T^{trig} of the trigger particle which we describe as

$$N_{\text{jet}} = N_{\text{jet}0} + d_N p_T^{\text{trig}}, \quad (24)$$

$$T_{\text{jet}} = T_{\text{jet}0} + d_T p_T^{\text{trig}}. \quad (25)$$

We also find that the width parameter R depends slightly on p_T which we can parametrize as

$$R = R_0 \frac{m_a}{\sqrt{m_a^2 + p_T^2}}. \quad (26)$$

Using this set of parameters and Eq. (23), we fit the

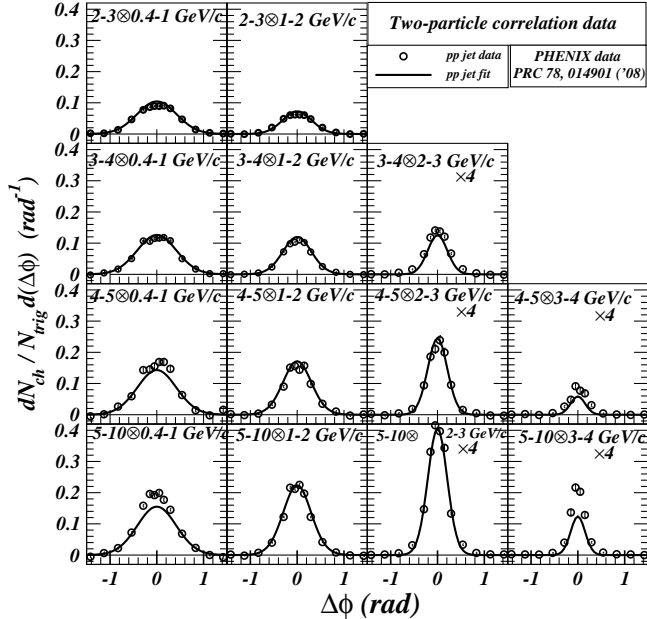


FIG. 6. PHENIX azimuthal angular distribution of associated particles per trigger in different $p_T^{\text{trig}} \otimes p_T^{\text{assoc}}$ combinations. The open circles are the associated particle yields per trigger, $dN_{\text{ch}}/N_{\text{trig}}d\Delta\phi$, in pp collisions [37]. The solid curves are the theoretical associated particle yields per trigger calculated with Eq. (23).

pp associated particle data obtained in PHENIX measurements for pp collisions at $\sqrt{s_{NN}} = 200$ GeV. The values of the parameters are given in Table III. As extracted from Fig. 1 of [43], the theoretical results of $dN_{\text{ch}}^{pp}/N_{\text{trig}}d\Delta\phi$ from Eq. (23) are given as solid curves in Fig. 6 and the corresponding experimental data are represented by open circles. As one observes in Fig. 6, although the fit is not perfect, the set of parameters in Table III adequately describe the set of pp associated particle data for $2 < p_T^{\text{trig}} < 10$ GeV and for $0.4 < p_T^{\text{assoc}} < 4$ GeV. As indicated in Table III, the parameters of Eqs. (24) and (25) are $N_{\text{jet}0} = 0.15$, $d_N = 0.1/\text{GeV}$, $T_{\text{jet}0} = 0.19$ GeV, and $d_T = 0.06$. It is interesting to note that the cone angle R_0 for jets in the lower- p_T region is of the same order as those in the high- p_T region.

The presence of a well-defined cone of particles associated with a $p_T > 2$ -3 GeV triggers in Fig. 6 on the near-side and the non-vanishing extrapolation of the jet yield N_{jet} to the case of a low- p_T trigger in Eq. (24) provide an additional evidence of jet production in the $p_T^{\text{trigger}} > 2$ GeV region in high energy pp collisions. Furthermore, even in minimum- p_T -biased events without a high- p_T trigger, a similar cone of associated correlated particles at $(\Delta\phi, \Delta\eta) \sim 0$ are present in two-particle correlation data, as shown in Fig. 7 [35, 38–40], indicating the production of jet-like structure on the near-side for low- p_T particles.

TABLE III. Jet component parameters in Eq. (23) obtained for the description of experimental near-side associated particles with different p_T^{trig} triggers in STAR [34] and PHENIX [37] Collaborations, in pp collisions at $\sqrt{s_{NN}}=200$ GeV.

	STAR	PHENIX			
p_T^{trig}	4-6 GeV	2-3 GeV	3-4 GeV	4-5 GeV	5-10 GeV
N_{jet}	0.75	$0.15 + 0.10 \langle p_T^{\text{trig}} \rangle / \text{GeV}$			
T_{jet}	0.55 GeV	$0.19 \text{ GeV} + 0.06 \langle p_T^{\text{trig}} \rangle$			
R_0	0.50				
m_a	1.1 GeV				

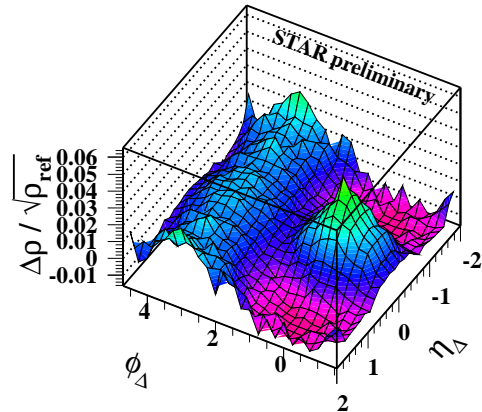


FIG. 7. (Color online) Minimum- p_T -biased two-particle angular correlation, without a p_T trigger selection, for charged hadrons produced in pp collisions at $\sqrt{s}=200$ GeV (from Fig. 1 of Ref. [39] of the STAR Collaboration). Here, ϕ_Δ is $\Delta\phi$, the difference of the azimuthal angles of two detected charged hadrons, and η_Δ is $\Delta\eta$, the difference of their pseudorapidities.

In addition to the particles associated with trigger particle on the near-side, there are particles associated with the trigger particle on the back-to-back, away-side at $\Delta\phi \sim \pi$, in the form of a ridge along the $\Delta\eta$ direction, both with high- p_T [34–36] and low- p_T triggers [35, 38–40], for pp collisions at $\sqrt{s} = 200$ GeV. Here, the importance of the production the low- p_T jet (minijets) in the low- p_T region has already been pointed out previously in the work of [38–41]. In Fig. 7, (taken from the STAR data in Fig. 1 of [39]), we show the two-particle correlation data in a minimum- p_T -biased measurements which corresponds to the case with a low- p_T trigger. The two-particle correlation data in Fig. 7 indicate the presence of (i) a near-side particle cluster at $(\Delta\phi, \Delta\eta) \sim 0$ (a mini-jet) and (ii) an away-side ridge of associated particles at $\Delta\phi \sim \pi$. The $\Delta\phi \sim \pi$ (back-to-back) correlation in the shape of a ridge indicates that the two particles are parts of the partons from the two nucleons and they carry fractions of the longitudinal momenta of their parents, leading to the ridge of $\Delta\eta$ at $\Delta\phi \sim \pi$. These two group of particles at $\Delta\phi \sim 0$ and $\Delta\phi \sim \pi$ can be interpreted as arising from the pair

of scattered partons in a relativistic hard scattering.

The dominance of the hard scattering in the spectrum does not imply the absence of soft processes. It only stipulates that the soft process contribution is much smaller in comparison. In the lowest p_T region, one expects contributions from soft nonperturbative QCD physics that may involve the parton wave functions in a flux tube [53], the thermodynamics and the recombination of partons [18, 54–56], or the fragmentation of a QCD string [57–59]. However, as the contributions from the hard-scattering processes increase with increasing collision energies, the fraction of the contributions from soft processes becomes smaller in comparison with the contributions from the hard-scattering processes, as pointed out earlier in [7, 32]. As a consequence, the contributions from the hard-scattering process can dominate the particle production process in high-energy pp and $p\bar{p}$ collisions.

VI. EFFECTS OF PARTON SHOWERING ON TRANSVERSE DIFFERENTIAL CROSS SECTION

The last sections show the possible dominance of jet production at central rapidity in high-energy pp and $p\bar{p}$ collisions over essentially the whole p_T region. We would like to find out how the jets evolve to become hadrons and how the hadron spectra manifest themselves.

In addition to the jet transverse spectra, experimental measurements also yield the hadron spectra without the reconstruction of jets. The hadron transverse spectra give a slightly greater power index, $n_{\text{hadron}} \sim 6-10$ [2, 9–14]. Previously, we outline how the increase in the power index n from jet production to hadron production may arise from the subsequent parton showering that turns jets into hadrons [12]. We would like to describe here the evolution in more details. To distinguish between jets and its shower products, we shall use the symbol c to label a parent parton jet and its momentum and the symbol p to label a shower product hadron and its momentum.

The evolution of the parton jet into hadrons by parton showering has been described well by many models [60]. There are three different parton showering schemes: the PYTHIA [61], the HERWIG [62], and the ARIADNE [63]. The general picture is that the initial parton is characterized by a momentum and a virtuality which measures the degree of the parton to be off-the-mass-shell. The parton is subject to initial-state and final-state radiations. After the hard scattering process, the parton possesses a high degree of virtuality $Q^{(0)}$, which can be identified with the magnitude of the parton transverse momentum c_T . The final-state radiation splits the parton into binary quanta as described by the following splitting

DGLAP kernels [64],

$$P_{q \rightarrow qg} = \frac{1}{3} \frac{1+z^2}{1-z}, \quad (27)$$

$$P_{g \rightarrow gg} = 3 \frac{[1-z(1-z)]^2}{z(1-z)}, \quad (28)$$

$$P_{g \rightarrow q\bar{q}} = \frac{n_f}{2} [z^2 + (1-z)^2], \quad (29)$$

where z is the momentum fraction of one of the showered partons, and there is symmetry between z and $1-z$ for symmetrical products in the second and third processes. After the showering splitting processes, there is always a leading parton with

$$z_{\text{leading}} \gg z_{\text{non-leading}}. \quad (30)$$

For the study of the p_T hadron spectra as a result of the parton showering, it suffices to focus attention on the leading parton after each showering splitting because of the rapid fall-off of the transverse momentum distribution as a function of increasing c_T . As a consequence, we can envisage the approximation conservation of the leading parton as the parton showering proceeds and as its momentum is degraded in each showering branching by the fraction $\langle z \rangle = \langle z_{\text{leading}} \rangle$. In the present study of high- p_T particles in the central rapidity region, the parton c is predominantly along the transverse direction, and the showering of the produced hadrons will also be along the transverse direction.

A jet parton c which evolves by parton showering will go through many generations of showering. If we label the (average) momentum of the i -th generation parton by $c_T^{(i)}$, the showering can be represented as $c_T \rightarrow c_T^{(1)} \rightarrow c_T^{(2)} \rightarrow c_T^{(3)} \rightarrow \dots \rightarrow c_T^{(\lambda)} = p_T$. Each branching will kinematically degrade the momentum of the showering parton by a momentum fraction, $\langle z \rangle = c_T^{(i+1)} / c_T^{(i)}$. At the end of the terminating λ -th generation of showering, the jet hadronizes and the p_T of a produced hadron is related to the c_T of the parent parton jet by

$$\frac{p_T}{c_T} \equiv \frac{c_T^{(\lambda)}}{c_T} = \langle z \rangle^\lambda. \quad (31)$$

It is easy to prove that if the generation number λ and the fragmentation fraction z are independent of the jet c_T , then the power law and the power index for the p_T distribution are unchanged [12].

We note however that in addition to the kinematic decrease of c_T as described by (31), the showering generation number λ is governed by an additional criterion on the virtuality. From the different parton showering schemes in the PYTHIA [61], the HERWIG [62], and the ARIADNE [63], we can extract the general picture that the initial parton with a large initial virtuality $Q^{(0)}$ decreases its virtuality by showering until a limit of Q^{cutoff} is reached. The downgrading of the virtuality will proceed as $Q^{\text{jet}} = Q^{(0)} \rightarrow Q^{(1)} \rightarrow Q^{(2)} \rightarrow Q^{(3)} \rightarrow \dots \rightarrow$

$Q^{(\lambda)}=Q^{\text{cutoff}}$, with

$$\langle \xi \rangle = \frac{Q^{(i+1)}}{Q^{(i)}} \quad \text{and} \quad \frac{Q^{(\lambda)}}{Q^{\text{jet}}} = \langle \xi \rangle^\lambda. \quad (32)$$

The measure of virtuality has been defined in many different ways in different parton showering schemes. We can follow PYTHIA [60] as an example. We consider a parton branching of $a \rightarrow bc$. The transverse momentum along the jet a direction is

$$b_T^2 = z(1-z)a^2 - (1-z)b^2 - zc^2. \quad (33)$$

If $a^2 = [Q^{(i)}]^2$ =virtuality before parton branching, and $b^2 = c^2 = 0$, as is assumed by PYTHIA, then

$$b_T^2 = [Q^{(i+1)}]^2 = z(1-z)a^2 = z(1-z)[Q^{(i)}]^2. \quad (34)$$

So, if we identify the transverse momentum b_T^2 along the jet axis as the square of virtuality $[Q^{(i+1)}]^2$ after parton branching, the quantity $z(1-z)$ measures the degradation of the square of the virtuality in each QCD branching process,

$$\frac{[Q^{(i+1)}]^2}{[Q^{(i)}]^2} = z(1-z). \quad (35)$$

Thus, the virtuality fraction of Eq. (32) is related to $\langle z(1-z) \rangle$ by

$$\langle \xi \rangle = \sqrt{\langle z(1-z) \rangle}. \quad (36)$$

As z is less than 1, $\langle \xi \rangle < \langle z \rangle$ which implies that on the average the virtuality fraction $\langle \xi \rangle$ in a parton branching is smaller than the momentum fraction $\langle z \rangle$. As a consequence, the virtuality of the leading parton is degraded faster than its momentum as the showering process proceeds so that when the virtuality reaches the cutoff limit, the parton still retains a significant fraction of the initial jet momentum.

The process of parton showering will be terminated when the virtuality $Q^{(\lambda)}$ reaches the cutoff value $Q^{(\lambda)}=Q^{\text{cutoff}}$, at which the parton becomes on-the-mass-shell and appears as a produced hadron. This occurs after λ generations of parton showering. The generation number λ is determined by

$$\lambda = \ln \left(\frac{Q^{\text{cutoff}}}{Q^{\text{jet}}} \right) / \ln \langle \xi \rangle. \quad (37)$$

There is a one-to-one mapping of the initial virtuality Q^{jet} with the initial jet transverse momentum c_T of the evolving parton as $Q^{\text{jet}}(c_T)$ (or conversely $c_T(Q^{\text{jet}})$). The cut-off virtuality Q^{cutoff} maps into a transverse momentum $c_{T0}=c_T(Q^{\text{cutoff}})$. Because of such a mapping, the decrease in virtuality Q corresponds to a decrease of the corresponding mapped c_T . We can infer from Eq. (37) an approximate relation between c_T and the number of generations, λ ,

$$\lambda = \ln \left(\frac{Q^{\text{cutoff}}(c_{T0})}{Q^{(0)}(c_T)} \right) / \ln \langle \xi \rangle \simeq \ln \left(\frac{c_{T0}}{c_T} \right) / \ln \langle \xi \rangle. \quad (38)$$

Thus, the showering generation number λ depends on the magnitude of the jet momentum c_T . On the other hand, kinematically, the showering processes degrades the transverse momentum of the parton c_T to that of the p_T of the produced hadron as given by Eq. (31), depending on the number of generations λ . The magnitude of the transverse momentum p_T of the produced hadron is related to the transverse momentum c_T of the parent parton jet by

$$\frac{p_T}{c_T} = \langle z \rangle^\lambda = \langle z \rangle^{\ln(c_{T0}/c_T)/\ln \langle \xi \rangle}. \quad (39)$$

We can solve the above equation for p_T as a function of c_T and obtain

$$\frac{p_T}{c_{T0}} = \left(\frac{c_T}{c_{T0}} \right)^{1-\mu}, \quad (40)$$

and conversely

$$\frac{c_T}{c_{T0}} = \left(\frac{p_T}{c_{T0}} \right)^{1/(1-\mu)}, \quad (41)$$

where

$$\mu = \frac{\ln \langle z \rangle}{\ln \langle \xi \rangle}. \quad (42)$$

In practice μ (or equivalently, the cut-off parameter Q^{cutoff} or c_{T0}) is a parameter that can be tuned to fit the data. As a result of the virtuality degradation and virtuality cut-off, the hadron fragment transverse momentum p_T is related to the parton momentum c_T nonlinearly by an exponent $1 - \mu$.

After the showering of the parent parton c_T to the produced hadron p_T , the hard-scattering cross section for the scattering in terms of hadron momentum p_T becomes

$$\frac{d^3\sigma(AB \rightarrow pX)}{dyd\mathbf{p}_T} = \frac{d^3\sigma(AB \rightarrow cX)}{dydc_T} \frac{dc_T}{d\mathbf{p}_T}. \quad (43)$$

Upon substituting the non-linear relation (41) between the parent parton moment c_T and the produced hadron p_T in Eq. (41), we get

$$\frac{dc_T}{d\mathbf{p}_T} = \frac{1}{1-\mu} \left(\frac{p_T}{c_{T0}} \right)^{\frac{2\mu}{1-\mu}}. \quad (44)$$

Therefore under the parton showering from c to p , the hard-scattering invariant cross section $\sigma_{\text{inv}}(p_T)$ for $AB \rightarrow pX$ for hadron production becomes

$$\begin{aligned} \sigma_{\text{inv}}(p_T) &= E_c \frac{d^3\sigma(AB \rightarrow pX)}{dp^3} \Big|_{y \sim 0} = \frac{d^3\sigma(AB \rightarrow pX)}{dyd\mathbf{p}_T} \Big|_{y \sim 0} \\ &\propto \frac{\alpha_s^2(Q^2(c_T))(1-x_{a0}(c_T))^{g_a+\frac{1}{2}}(1-x_{b0}(c_T))^{g_b+\frac{1}{2}}}{p_T^{n'} \sqrt{1-x_c(c_T)}}, \end{aligned} \quad (45)$$

where

$$n' = \frac{n-2\mu}{1-\mu}, \quad \text{with } n = 4 + \frac{1}{2}. \quad (46)$$

Thus, the power index n for jet production can be significantly changed to n' for hadron production because the greater the value of the parent jet c_T , the greater the number of generations λ to reach the produced hadron, and the greater is the kinematic energy degradation. By a proper tuning of μ , the power index can be brought to agree with the observed power index n' in hadron production. The quantity μ is related to n' and n by

$$\mu = \frac{n' - n}{n' - 2} \quad (47)$$

For example, for $\mu=0.4$ one gets $n'=6.2$ and for $\mu = 0.6$ one gets $n'=8.2$.

VII. REGULARIZATION AND FURTHER APPROXIMATION OF THE HARD-SCATTERING INTEGRAL

In order to apply the power-law (45) to the whole range of p_T for hadron production, we need to regularize it. Upon choosing the regularization (21), the differential invariant cross section $\sigma_{\text{inv}}(p_T)$ for the production of a hadron with a transverse momentum p_T becomes

$$\sigma_{\text{inv}}(p_T) = \left. \frac{d^3\sigma(AB \rightarrow pX)}{dyd\mathbf{p}_T} \right|_{y \sim 0} \propto \frac{\alpha_s^2(Q^2(c_T))(1 - x_{a0}(c_T))^{g_a + \frac{1}{2}}(1 - x_{b0}(c_T))^{g_b + \frac{1}{2}}}{(1 + m_T/m_{T0})^{n'}\sqrt{1 - x_c(c_T)}}. \quad (48)$$

In the above equation, the variable $c_T(p_T)$ on the right-hand side refers to the transverse momentum of the parent jet c_T before parton showering as given by Eq. (41),

$$\frac{c_T(p_T)}{c_{T0}} = \left(\frac{p_T}{c_{T0}} \right)^{(n'-2)/(n-2)}. \quad (49)$$

The quantities x_{a0} , x_{b0} , and x_c in Eqs. (45) are given by Eq. (5).

We can simplify further the p_T dependencies of the structure function in Eq. (48) and the running coupling constant as additional power indices in such a way that will facilitate subsequent phenomenological comparison. We can cast the hard-scattering integral Eq. (48) for hadron production in the nonextensive statistical mechanical distribution form

$$\left. \frac{d^3\sigma(AB \rightarrow pX)}{dyd\mathbf{p}_T} \right|_{y \sim 0} = \sigma_{\text{inv}}(p_T) \sim \frac{A}{[1 + m_T/m_{T0}]^n}, \quad (50)$$

where

$$n = n' + n_\Delta, \quad (51)$$

and n' is the power index after taking into account the parton showering process, n_Δ the power index from the structure function and the coupling constant. We consider the part of the p_T -dependent factor in Eq. (48)

$$f(p_T) = \frac{\alpha_s^2(c_T(p_T))(1 - 2c_T(p_T)/\sqrt{s})^{g_a + g_b + 1}}{[1 - c_T(p_T)/\sqrt{s}]^{1/2}} \quad (52)$$

that is a known function of p_T . We wish to match it to a nonextensive statistical mechanical distribution with a power index n_Δ ,

$$\tilde{f}(p_T) = \frac{\tilde{A}}{(1 + m_T(p_T)/m_{T0})^{n_\Delta}}. \quad (53)$$

We match the two functions at two points, p_{T1} and p_{T2} ,

$$f(p_{Ti}) = \tilde{f}(p_{Ti}), \quad i = 1, 2 \quad (54)$$

Then we get

$$n_\Delta = \frac{\ln f(p_{T1}) - \ln f(p_{T2})}{\ln(1 + m_T(p_{T2})/m_{T0}) - \ln(1 + m_T(p_{T1})/m_{T0})}. \quad (55)$$

As $f(p_T)$ is a known function of p_T and \sqrt{s} , n_Δ can in principle be determined. The total power index n as given by (51) is also a function of \sqrt{s} .

In reaching the above representation of Eq. (50) for the invariant cross section for hadrons, we have approximated the hard-scattering integral $\sigma_{\text{inv}}(p_T)$ that may not be exactly in the form of $A/[1 + m_T/m_{T0}]^n$ into such a form. It is easy then to see that the upon matching $\sigma_{\text{inv}}(p_T)$ with $A/[1 + m_T/m_{T0}]^n$ according to some matching criteria, the hard-scattering integral $\sigma_{\text{inv}}(p_T)$ will be in excess of $A/[1 + m_T/m_{T0}]^n$ in some region, and is in deficit in some other region. As a consequence, the ratio of the hard-scattering integral $\sigma_{\text{inv}}(p_T)$ to the fitting $A/[1 + m_T/m_{T0}]^n$ will oscillate as a function of p_T . This matching between the physical hard-scattering outcome that contains all physical effects with the approximation of Eq. (50) may be one of the origins of the oscillations of the experimental fits with the nonextensive distribution (as can be seen below in Fig. 8).

VIII. SINGLE-PARTICLE NONEXTENSIVE DISTRIBUTION AS A LOWEST-ORDER APPROXIMATION OF THE HARD-SCATTERING INTEGRAL

In the hard-scattering integral Eq. (50) for hadron invariant cross section at central rapidity, if we identify

$$n \rightarrow \frac{1}{q-1} \quad \text{and} \quad m_{T0} \rightarrow \frac{T}{q-1} = nT, \quad (56)$$

and consider produced particles to be relativistic so that $m_T \sim E_T \sim p_T$, then we will get the nonextensive distribution of Eq. (1) as the lowest-order approximation for the QCD-based hard-scattering integral.

It is necessary to keep in mind that the outlines leading to Eqs. (48) and (50) pertains only to average values, as the stochastic elements and distributions of various quantities have not been properly taken into account. The convergence of Eq. (50) and Eq. (1) can be considered from a broader viewpoint of the reduction of a microscopic description to a single-particle statistical-mechanical description. From the microscopic perspective, the hadron production in a pp collision is a very

complicated process, as evidenced by the complexity of the evolution dynamics in the evaluation of the p_T spectra in explicit Monte Carlo programs, for example, in [61–63]. There are stochastic elements in the picking of the degree of inelasticity, in picking the colliding parton momenta from the parent nucleons, the scattering of the partons, the showering evolution of scattered partons, the hadronization of the fragmented partons. Some of these stochastic elements cannot be definitive and many different models have been put forth. In spite of all these complicated stochastic dynamics, the final result of Eq. (50) of the single-particle distribution can be approximated to depend only on three degrees of freedom, after all is done, put together, and integrated. The simplification can be considered as a “no hair” reduction from the microscopic description to nonextensive statistical mechanics in which all the complexities in the microscopic description “disappear” and subsumed behind the stochastic processes and integrations. In line with statistical mechanics and in analogy with the Boltzmann-Gibbs distribution, we can cast the hard-scattering integral in the nonextensive form in the lowest-order approximation as [15]⁴

$$\left. \frac{d\sigma}{dy d\mathbf{p}_T} \right|_{y \sim 0} = \frac{1}{2\pi p_T} \left. \frac{d\sigma}{dy dp_T} \right|_{y \sim 0} = A e_q^{-E_T/T}, \quad (57)$$

where

$$e_q^{-E_T/T} \equiv [1 - (1 - q) E_T/T]^{1/(1-q)},$$

$$e_1^{-E_T/T} = e^{-E_T/T}.$$

In the above equation, $E_T = \sqrt{m^2 + \mathbf{p}_T^2}$, where m can be taken to be the pion mass m_π , and we have assumed boost-invariance in the region near $y \sim 0$. The parameter q is related physically to the power index n of the spectrum, and the parameter T related to m_{T0} and the average transverse momentum, and the parameter A related to the multiplicity (per unity rapidity) after integration over p_T . Given a physically determined invariant cross section in the log-log plot of the cross section as a function of the transverse hadron energy as in Fig. 1, the slope at large p_T gives approximately the power index n (and q), the average of E_T is proportional to T (and m_{T0}), and the integral over p_T gives A .

We can test the above single-particle nonextensive statistical mechanical description by confronting Eq. (57) with experimental data. Fig. 8 gives the comparisons of the results from Eq. (57) with the experimental p_T spectra at central rapidity obtained by different Collaborations [65–68]. In these calculations, the parameters of A , q and the corresponding n and T are given in Table III. The dashed line (an ordinary exponential of E_T for

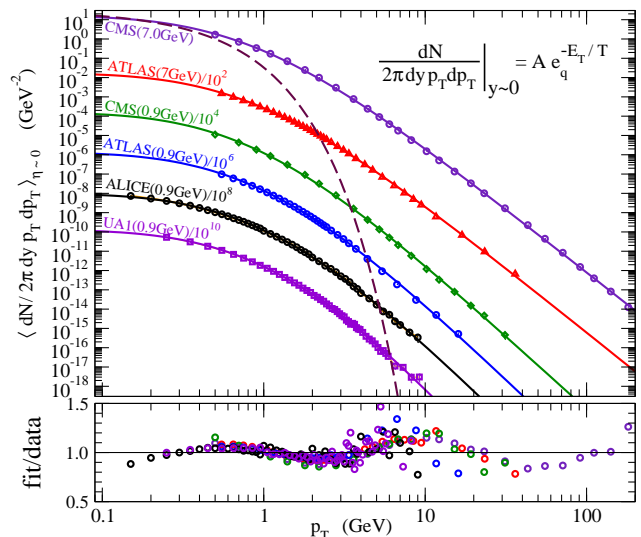


FIG. 8. (Color online) Comparison of Eq. (57) with the experimental transverse momentum distribution of hadrons in pp collisions at central rapidity y . The corresponding Boltzmann-Gibbs (purely exponential) distribution is illustrated as the dashed curve. For a better visualization, both the data and the analytical curves have been divided by a constant factor as indicated. The ratios data/fit are shown at the bottom, where a roughly log-periodic behavior is observed on top of the q -exponential one. Data are taken from [65–68].

$q \rightarrow 1$) illustrates the large discrepancy if the distribution is described by Boltzmann-Gibbs distribution. The results in Fig. 8 shows that Eq. (57) adequately describes the hadron p_T spectra at central rapidity in high-energy pp collisions. We verify that q increases slightly with the beam energy, but, for the present energies, remains always $q \simeq 1.1$, corresponding to a power index n in the range of 6-10 that decreases as a function of \sqrt{s} .

TABLE IV. Parameters used to obtain fits presented in Fig. 8. The values of A is in units of GeV^{-2}/c^3 .

Collaboration	\sqrt{s}	A	q	$n=1/(q-1)$	$T(\text{GeV})$
CMS [65]	pp at 7TeV	16.2	1.151	6.60	0.147
ATLAS[66]	pp at 7TeV	17.3	1.148	6.73	0.150
CMS [65]	pp at 0.9TeV	15.8	1.130	7.65	0.128
ATLAS[66]	pp at 0.9TeV	13.6	1.124	8.09	0.140
ALICE[67]	pp at 0.9TeV	9.95	1.119	8.37	0.150
UA1 [68]	$\bar{p}p$ at 0.9TeV	13.1	1.109	9.21	0.154

What interestingly emerges from the analysis of the data in high-energy pp collisions is that the good agreement of the present phenomenological fit extends to the whole p_T region (or at least for p_T greater than 0.2 GeV/ c , where reliable experimental data are available) [11]. This is being achieved with a single nonextensive statistical mechanical distribution with only three degrees of freedom with data-to-fit ratios oscillating about unity as in Fig. 8. Such an agreement suggests that the nonextensive statistical mechanical distribution

⁴ We are adopting the convention of unity for both the Boltzmann constant k_B and the speed of light c .

may not only be the phenomenological description of the end product of the parton showering evolution from jet to hadrons but may have deeper theoretical significance.

IX. SUMMARY AND DISCUSSIONS

Transverse momentum distribution of jets and hadrons provide complementary and useful pieces of information on the collision mechanisms and their evolution dynamics. The spectra of jets reveal the simple hard-scattering production mechanism and they carry the distinct signature with a power index of $n \sim 4 - 5$. On the other hand, the spectra of hadrons contain additional subsequent dynamics on the evolution of jets into hadrons but retain the power-law feature of the hard-scattering process. Recent description of the hadron transverse spectrum by a single nonextensive statistical mechanical distribution leads to the suggestion of the possible dominance of the hard-scattering process, not only in the high p_T region, but also over essentially the whole p_T region, for pp and $\bar{p}p$ collisions. The suggestion represents a synthesizing description linking the simplicity of the whole hadron spectrum for pp collisions with the production of minijets [7] at p_T of a few GeV and the production of minijets at low- p_T [38–41] into a single simplifying observation on the dominance of the hard-scattering over the whole p_T region in pp collisions, with a special emphasis on the production mechanism.

We have searched for direct supporting evidences for the dominance of the hard-scattering process in the whole p_T region at central rapidity. The first piece of evidence has been found by studying the power index for jet production in the lower- p_T region in the UA1 and ATLAS data in high-energy $\bar{p}p$ and pp collisions, where the power index is indeed close to 4 - 5, the signature of pQCD jet production. The dominance of the hard-scattering process for the production of low- p_T hadron in the central rapidity region is further supported by two-particle correlation data where associated particles are correlated on the near-side at $(\Delta\phi, \Delta\eta) \sim 0$, with a minimum- p_T -biased or a high- p_T trigger, indicating the production of angular clusters in essentially the whole range of p_T . Additional evidence has been provided by the two-particle correlation on the away-side at $\Delta\phi \sim \pi$, with a minimum- p_T -biased or a high- p_T trigger, where a produced hadron has been found to correlate with a “ridge” of particles along $\Delta\eta$ [35, 38–41]. The $\Delta\phi \sim \pi$ correlation indicates that the correlated pair is related by a collision, and the $\Delta\eta$ correlation in the shape of a ridge indicates that the two particles are partons from the two nucleons and they carry different fractions of the longitudinal momenta of their parents, leading to the ridge of $\Delta\eta$ at $\Delta\phi \sim \pi$.

Hadron production in high-energy pp and $\bar{p}p$ collisions are complex processes. They can be viewed from two different and complementary perspectives. On the one hand, there is the successful microscopic description involving perturbative QCD and nonperturbative

hadronization at the parton level where one describes the detailed mechanisms of parton-parton hard scattering, parton structure function, parton fragmentation, parton showering, the running coupling constant and other QCD processes [6]. On the other hand, from the viewpoint of statistical mechanics, the single-particle distribution may be cast into a form that exhibit all the essential features of the process with only three degrees of freedom [11, 12, 15]. The final result of the process may be summarized, in the lowest-order approximation, by a power index n which can be represented by a nonextensivity parameter $q=(n+1)/n$, the average transverse momentum m_{T0} which can be represented by an effective temperature $T=m_{T0}/n$, and a constant A that is related to the multiplicity per unit rapidity when integrated over p_T . We have successfully confronted such a phenomenological nonextensive statistical mechanical description with experimental data. We emphasize also that, *in all cases*, the temperature turns out to be close to the mass of the pion.

What we may extract from the behavior of the experimental data is that scenario proposed in [18, 19] appears to be essentially correct excepting for the fact that we are not facing thermal equilibrium but a different type of stationary state, typical of violation of ergodicity (for a discussion of the kinetic and effective temperatures see [69, 70]; a very general discussion of the notion of temperature on nonextensive environments can be found in [71]). It should be realized however that the connection between the power law and the nonextensive statistical mechanical description we have presented constitutes only a plausible mathematical outline and an approximate roadmap. It will be of interest in future work to investigate more rigorously the stochastic parton showering process from a purely statistical mechanical viewpoint to see how it can indeed lead to a nonextensive statistical distribution by deductive, physical, and statistical principles so that the underlying nonextensive parameters can be determined from basic physical quantities of the collision process.

We can discuss the usefulness of our particle production results in pp collisions in relation to particle production in AA collisions. In the lowest approximation with no initial-state and final-state interactions, an AA collision at a certain centrality \mathbf{b} can be considered as a collection of binary $N_{\text{bin}}(\mathbf{b})$ number of pp collisions. These binary collisions lead first to the production of primary particles. Successive secondary and tertiary collisions between primary particles lead to additional contributions

in a series:

$$\begin{aligned} \frac{E_p dN^{AA}}{d\mathbf{p}}(\mathbf{b}, \mathbf{p}) &= N_{\text{bin}}(\mathbf{b}) \frac{E_p dN^{pp}}{d\mathbf{p}}(\mathbf{p}) \\ &+ N_{\text{bin}}^2(\mathbf{b}) \int d\mathbf{p}_1 d\mathbf{p}_2 \frac{dN^{pp}}{d\mathbf{p}_1} \frac{dN^{pp}}{d\mathbf{p}_2} \frac{E_p dN(\mathbf{p}_1 \mathbf{p}_2 \rightarrow \mathbf{p} X')}{d\mathbf{p}} \\ &+ N_{\text{bin}}^3(\mathbf{b}) \int d\mathbf{p}_1 d\mathbf{p}_2 d\mathbf{p}_3 \frac{dN^{pp}}{d\mathbf{p}_1} \frac{dN^{pp}}{d\mathbf{p}_2} \frac{dN^{pp}}{d\mathbf{p}_3} \\ &\quad \times \frac{E_p dN(\mathbf{p}_1 \mathbf{p}_2 \mathbf{p}_3 \rightarrow \mathbf{p} X')}{d\mathbf{p}} + \dots \end{aligned} \quad (58)$$

where $E_p dN(\mathbf{p}_1 \mathbf{p}_2 \dots \rightarrow \mathbf{p} X')/d\mathbf{p}$ is the particle distribution of \mathbf{p} after binary collisions of primary particles $\mathbf{p}_1, \mathbf{p}_2, \dots$. In addition to the primary products of a single relativistic hard-scattering $E dN^{pp}/d\mathbf{p}$ represented by the first term on the right-hand side, the spectrum in AA collisions contains contributions from secondary and tertiary products represented by the second and third terms. In the next level of approximation, additional initial-state and final-state interactions will lead to further modifications of the ratio $R_{AA} = dN^{AA}/[N_{\text{bin}} dN^{pp}]$ as a function of \mathbf{b} and \mathbf{p}_T .

The usefulness of our analysis arises from a better understanding of the plausible reasons why the products from the primary pp scattering can be simply represented by a single nonextensive statistical mechanical distribution (57). For peripheral collisions, the first term of Eq. (58) suffices and the spectrum of AA collision, normalized per binary collision, would be very similar to that of the pp collision, as is indeed the case in Fig. 1 of [72]. As the number of binary collisions increases in more central collisions, the second term becomes important and shows up as an additional component of nonextensive statistical mechanical distribution with a new set of n and T parameters in the region of low p_T , as discussed in [73, 74].

As a concluding remark, we note that the data/fit plot in the bottom part of Fig. 8 exhibit an intriguing rough log-periodicity oscillations, which suggest corrections to the lowest-order approximation of Eq. (57) and some hierarchical fine-structure in the quark-gluon system where hadrons are generated. This behavior is possibly an indication of some kind of fractality in the system. Indeed, the concept of *self-similarity*, one of the landmarks of fractal structures, has been used by Hagedorn in his definition of fireball, as was previously pointed out in [21] and found in analysis of jets produced in pp collisions at LHC [75]. This small oscillations have already been preliminary discussed in Section 8 and in [76, 77], where the authors were able to mathematically accommodate these observed oscillations essentially allowing the index q in the very same Eq. (57) to be a complex number⁵ (see also Refs. [78, 79]; more details on this phenomenon, including also discussion of its presence in recent AA data, can be found in [80]).

Acknowledgements

One of the authors (CYW) would like to thank Dr. Xin-Nian Wang for helpful discussions. The research of CYW was supported in part by the Division of Nuclear Physics, U.S. Department of Energy under Contract DE-AC05-00OR22725, and the research of GW was supported in part by the National Science Center (NCN) under contract Nr 2013/08/M/ST2/00598 (Polish agency). Two of us (L.J.L.C. and C.T.) have benefited from partial financial support from CNPq, Faperj and Capes (Brazilian agencies). One of us (CT) acknowledges partial financial support from the John Templeton Foundation.

-
- [1] R. Blankenbecler and S. J. Brodsky, Phys. Rev. D **10**, 2973 (1974); R. Blankenbecler, S. J. Brodsky and J. Gunion, Phys. Rev. D **12**, 3469 (1975); E. A. Schmidt and R. Blankenbecler, Phys. Rev. D **15**, 332 (1977); R. Blankenbecler, Lectures presented at Tübingen University, Germany, June 1977, SLAC-PUB-2077 (1977).
[2] A.L.S. Angelis *et al.* (CCOR Collaboration), Phys. Lett. B **79**, 505 (1978).
[3] R. P. Feynman, R. D. Field and G. C. Fox, Phys. Rev. D **18**, 3320 (1978).
[4] J. F. Owens, E. Reya, and M. Glöck, Phys. Rev. D **18**, 1501 (1978).
[5] D. W. Duke, J. F. Owens, Phys. Rev. D **30**, 49 (1984).
[6] T. Sjöstrand and M. van Zijl, Phys. Rev. D **36**, 2019 (1987); R. Corke and T. Sjöstrand, JHEP

- 1103**, 032 (2011) [arxiv : 1011.1759]; T. Sjöstrand and P. Z. Skands, Eur. Phys. J. C **39**, 129 (2005), [arXiv:hep-ph/0408302]; T. Sjöstrand and P. Z. Skands, JHEP **03**, 053 (2004), [arXiv:hep-ph/0402078].
[7] X.N. Wang and M. Gyulassy, Phys. Rev. D **44**, 3501 (1991) and Phys. Rev. D **45**, 734 (1992).
[8] C. Y. Wong, *Introduction to High-Energy Heavy-Ion Collisions*, World Scientific Publisher, 1994.
[9] J. Rak and M. J. Tannenbaum, *High- p_T Physics in the Heavy Ion*, Cambridge University Press, Cambridge, 2013.
[10] F. Arleo, S. Brodsky, D. S. Hwang and A. M. Sickles, Phys. Rev. Lett. **105**, 062002 (2010).
[11] C. Y. Wong and G. Wilk, Acta Phys. Pol. B **43**, 2047 (2012).
[12] C. Y. Wong and G. Wilk, Phys. Rev. D **87**, 114007 (2013).
[13] C. Y. Wong, G. Wilk, *Relativistic Hard-Scattering and Tsallis Fits to p_T Spectra in pp Collisions at the LHC*, arXiv:1309.7330[hep-ph]
[14] C.-Y. Wong, G. Wilk, L. J. L. Cirto and C. Tsallis; EPJ

⁵ It should be noted here that other alternative to complex q would be log-periodic fluctuating scale parameter T , such possibility was discussed in [77].

- Web of Conf. **90**, 04002 (2015), arXiv:1412.0474.
- [15] L. J. L. Cirto, C. Tsallis, C.-Y. Wong and G. Wilk, *The transverse-momenta distributions in high-energy pp collisions - A statistical-mechanical approach*, arXiv:1409.3278 [hep-ph].
- [16] C. Tsallis, J. Stat. Phys. **52**, 479 (1988) and Eur. Phys. J. A **40**, 257 (2009); M. Gell-Mann and C. Tsallis eds., *Nonextensive Entropy - Interdisciplinary Applications* (Oxford University Press, New York, 2004). Cf. also C. Tsallis, *Introduction to Nonextensive Statistical Mechanics - Approaching A Complex World*, Springer, New York, 2009. A regularly updated bibliography on nonadditive entropies and nonextensive statistical mechanics is available at <http://tsallis.cat.cbpf.br/biblio.htm>.
- [17] C. Tsallis, Contemporary Physics, **55**, 179 (2014).
- [18] R. Hagedorn, Riv. Nuovo Cimento **6**, 1 (1983).
- [19] C. Michael and L. Vanryckeghem, J. Phys. G **3**, L151 (1977); C. Michael, Prog. Part. Nucl. Phys. **2**, 1 (1979).
- [20] I. Bediaga, E. M. F. Curado and J. M. de Miranda, Physica A **286**, 156 (2000);
- [21] C. Beck, Physica A **286**, 164 (2000).
- [22] M. Rybczyński, Z. Włodarczyk and G. Wilk, Nucl. Phys. B (Proc. Suppl.) **97**, 81 (2001); F. S. Navarra, O. V. Utyuzh, G. Wilk and Z. Włodarczyk, Phys. Rev. D **67**, 114002 (2003); G. Wilk and Z. Włodarczyk, J. Phys. G **38** 065101 (2011), Eur. Phys. J. A **40**, 299 (2009) and Eur. Phys. J. A **48**, 161 (2012), Cent. Eur. J. Phys. **10**, 568 (2012); M. Rybczyński, Z. Włodarczyk and G. Wilk, J. Phys. G **39**, 095004 (2012); M. Rybczyński and Z. Włodarczyk, Eur. Phys. J. C **74**, 2785 (2014).
- [23] K. Ürmösy, G. G. Barnaföldi and T. S. Biró, Phys. Lett. B **701**, 111 (2012), and B **718** 125 (2012); T.S. Biró, G.G. Barnaföldi and P. Ván, Eur. Phys. J. A **49**, 110 (2013) and Physica A **417**, 215 (2015); T. S. Biró, P. Ván, G. G. Barnaföldi and K. Ürmösy, Entropy **16**, 6497 (2014).
- [24] J. Cleymans and D. Worku, J. Phys. G **39**, 025006 (2012) and Eur. Phys. J. A **48**, 160 (2012); M. D. Azmi and J. Cleymans, J. Phys. G **41** 065001 (2014); L. Marques, J. Cleymans, and A. Deppman, Phys. Rev. D **91**, 054025 (2015).
- [25] A. Deppman, Physica A **391**, 6380 (2012) and J. Phys. G **41**, 055108 (2014); I. Sena and A. Deppman, Eur. Phys. J. A **49**, 17 (2013). A. Deppman, L. Marques, E. Andrade-II and A. Deppman, Phys. Rev. D **87**, 114022 (2013); W. Megias, D. P. Menezes and A. Deppman, Physica A **421**, 15 (2015).
- [26] P. K. Khandai, P. Sett, P. Shukla and V. Singh, Int. J. Mod. Phys. A **28**, 1350066 (2013) and J. Phys. G **41**, 025105; Bao-Chun Li, Ya-Zhou Wang and Fu-Hu Liu, Phys. Lett. B **725**, 352 (2013); T. Wibig, J. Phys. G **37**, 115009 (2010) and Eur. Phys. J. C **74**, 2966 (2014).
- [27] D. B. Walton and J. Rafelski, Phys. Rev. Lett. **84**, 31 (2000).
- [28] G. Wilka and Z. Włodarczyk, Entropy **17**, 384 (2015) and *Quasi-power law ensembles*, arXiv:1501.01936, to be published in Acta Phys. Pol. **B** (2015).
- [29] B. Abbott *et al.* (D0 Collaboration), Phys. Rev. D **64**, 032003 (2001).
- [30] B. Abelev *et al.* (ALICE Collaboration), Phys. Lett. B **722**, 262 (2013).
- [31] S. Chatrchyan *et al.* (CMS Collaboration), Phys. Rev. Lett. **107**, 132001 (2011).
- [32] C. Albajar *et al.* (UA1 Collaboration), Nucl. Phys. B **309**, 405 (1988).
- [33] G. Aad *et al.* (ATLAS Collaboration), Phys. Rev. D **84**, 054001 (2011).
- [34] J. Adams *et al.* (STAR Collaboration), Phys. Rev. Lett. **95**, 152301 (2005).
- [35] J. Adams *et al.* (STAR Collaboration), Phys. Rev. C **73**, 064907 (2006).
- [36] J. Putschke (STAR Collaboration), J. Phys. G **34**, S679 (2007).
- [37] A. Adare, *et al.* (PHENIX Collaboration), Phys. Rev. C **78**, 014901 (2008); Phys. Rev. D **83**, 052004 (2011) and Phys. Rev. C **83**, 064903 (2011).
- [38] J. Adams *et al.* (STAR Collaboration), Phys. Rev. C **74**, 032006 (2006).
- [39] R. J. Porter and T. A. Trainor, (STAR Collaboration), J. Phys. Conf. Ser. **27**, 98 (2005).
- [40] T. A. Trainor and R. L. Ray, Phys. Rev. C **84**, 034906 (2011).
- [41] R. L. Ray, Phys. Rev. D **84**, 034020 (2011); T. A. Trainor and D. J. Prindle, *Improved isolation of the p-p underlying event based on minimum-bias trigger-associated hadron correlations*, arXiv:1310.0408 [hep-ph].
- [42] C. Y. Wong, Phys. Rev. C **78**, 064905 (2008).
- [43] C. Y. Wong, Phys. Rev. C **80**, 034908 (2009).
- [44] C. Y. Wong, H. Wang, Phys. Rev. C **58**, 376 (1998).
- [45] R. Gastman and T. T. Wu, *The Ubiquitous Photon*, Clarendon Press, Oxford, 1990.
- [46] K. Kastella, Phys. Rev. D **36**, 2734 (1987).
- [47] G. Calucci and D. Treleani, Phys. Rev. D **41**, 3367 (1990), **44**, 2746 (1990), D **49**, 138 (1994), D **50**, 4703 (1994), D **63**, 116002 (2001); Int. Jour. Mod. Phys. A **6**, 4375 (1991); A. Accardi and D. Treleani, Phys. Rev. D **64**, 116004 (2001).
- [48] M. Gyulassy, P. Levai and I. Vitev, Nucl. Phys. B **594**, 371 (2001).
- [49] R. Corke and T. Sjöstrand, JHEP **1001**, 035 (2010).
- [50] J. Beringer *et al.*, (Particle Data Group), Phys. Rev. D **86**, 010001 (2012).
- [51] C. Y. Wong, E. S. Swanson and T. Barnes, Phys. Rev. C, **65**, 014903 (2001).
- [52] S. Chekanov *et al.*, (ZEUS Collaboration), Phys. Rev. D **67**, 012007 (2003) and Eur. Phys. J. **C42**, 1 (2005).
- [53] G. Gatoff and C. Y. Wong, Phys. Rev. D **46**, 997 (1992); C. Y. Wong and G. Gatoff, Phys. Rep. **242** 1994, 489 (1994).
- [54] R. Hagedorn and K. Redlich, Z. Phys. C **26**, 541 (1985).
- [55] I. Kraus, J. Cleymans, H. Oeschler and K. Redlich, Phys. Rev. C **79**, 014901 (2009).
- [56] R. C. Hwa and C. B. Yang, Phys. Rev. C **67** 034902 (2003) and Phys. Rev. C **75**, 054904 (2007); R. C. Hwa and Z. G. Tan, Phys. Rev. C **72**, 057902 (2005); C. B. Chiu and R. C. Hwa, Phys. Rev. C **72**, 034903 (2005) and Phys. Rev. C **79**, 034901 (2009); R. C. Hwa, Phys. Lett. B **666**, 228 (2008).
- [57] J. Schwinger, Phys. Rev. **82**, 664 (1951).
- [58] B. Andersson, G. Gustafson, and T. Sjöstrand, Zeit. für Phys. C **20**, 317 (1983); B. Andersson, G. Gustafson, G. Ingelman, and T. Sjöstrand, Phys. Rep. **97**, 31 (1983); T. Sjöstrand and M. Bengtsson, Computer Physics Comm. **43**, 367 (1987); B. Andersson, G. Gustafson, and B. Nilsson-Alqvist, Nucl. Phys. B **281**, 289 (1987).
- [59] R. C. Wang and C. Y. Wong, Phys. Rev D **38**, 348 (1988).
- [60] T. Sjöstrand and P. Z. Skands, Eur. Phys. J. C **39**, 129 (2005).

- [61] M. Bengtsson and T. Sjöstrand, Nucl. Phys. B **289**, 810 (1987); E. Norrbin and T. Sjöstrand, Nucl. Phys. B **603**, 297 (2001).
- [62] G. Marchesini and B. R. Webber, Nucl. Phys. B **238**, 1 (1984); G. Corcella, I. G. Knowles, G. Marchesini, S. Moretti, K. Odagiri, P. Richardson, M. H. Seymour, B. R. Webber, JHEP **01**, 010 (2001).
- [63] G. Gustafson, Phys. Lett. B **175**, 453 (1986); G. Gustafson, U. Pettersson, Nucl. Phys. B **306**, 746 (1988); L. Lönnblad, Computer Physics Commun. **71**, 15 (1992).
- [64] V. N. Gribov and L. N. Lipatov, Sov. J. Nucl. Phys. **15**, 75 (1972) and Sov. J. Nucl. Phys. **15**, 438 (1972); G. Altarelli and G. Parisi, Nucl. Phys. B **126**, 298 (1977); Yu. L. Dokshitzer, Sov. J. Phys. JETP **46**, 641 (1977).
- [65] V. Khachatryan *et al.* (CMS Collaboration), JHEP **02**, 041 (2010) and JHEP **08**, 086 (2011), Phys. Rev. Lett. **105**, 022002 (2010).
- [66] G. Aad *et al.* (ATLAS Collaboration), New J. Phys. **13**, 053033 (2011).
- [67] K. Aamodt *et al.* (ALICE Collaboration), Phys. Lett. B **693**, 53 (2013) and Eur. Phys. J. C **71**, 2662 (2013).
- [68] C. Albajar *et al.* (UA1 Collaboration), Nucl. Phys. B **335**, 261 (1990).
- [69] W. Niedenzu, T. Grieser and H. Ritsch, Europhys. Lett. **96**, 43001 (2011); L. A. Gougam and M. Tribeche, Phys. Plasmas **18**, 062102 (2011); L. A. Rios, R. M. O. Galvão, and L. Cirto, Phys. Plasmas **19**, 034701 (2012); L. J. L. Cirto, V. R. V. Assis, C. Tsallis, Physica A **393**, 286 (2014); H. Christodoulidi, C. Tsallis and T. Bountis, Europhys. Lett. **108**, 40006 (2014).
- [70] J. S. Andrade Jr., G. F. T. da Silva, A. A. Moreira, F. D. Nobre, E. M. F. Curado, Phys. Rev. Lett. **105**, 260601 (2010); M. S. Ribeiro, F. D. Nobre and E. M. F. Curado, Eur. Phys. J. B **85**, 399 (2012) and Phys. Rev. E **85**, 021146 (2012); E. M. F. Curado, A. M. C. Souza, F. D. Nobre and R. F. S. Andrade, Phys. Rev. E **89**, 022117 (2014).
- [71] T. S. Biró, *Is there a Temperature? Conceptual Challenges at High Energy, Acceleration and Complexity*, (Springer, New York Dordrecht Heidelberg London, 2011).
- [72] B. Abelev *et al.* (ALICE Collaboration), Phys. Lett. B **720**, 52 (2013).
- [73] K. Ürmösy, T. S. Biró, G. G. Barnaföldi and Z. Xu, *Disentangling Soft and Hard Hadron Yields in PbPb Collisions at $\sqrt{s_{NN}} = 2.76$ ATeV*, arXiv:1405.3963 (2014); K. Ürmösy, G. G. Barnaföldi, Sz. Harangozó, T. S. Biró and Z. Xu, *A soft + hard model for heavy-ion collisions*, arXiv:1501.02352.
- [74] M. Rybczyński, G. Wilk and Z. Włodarczyk, EPJ Web of Conf. **90**, 01002 (2015), arXiv:1411.5148.
- [75] G. Wilk and Z. Włodarczyk, Phys. Lett. B **727**, 163 (2013).
- [76] G. Wilk and Z. Włodarczyk, Physica A **413**, 53 (2014).
- [77] G. Wilk and Z. Włodarczyk, *Log-periodic oscillations of transverse momentum distributions*, arXiv:1403.3508 [hep-ph] (unpublished) and *Quasi-power laws in multiparticle production processes* arXiv:1503.08704v1 [hep-ph], to be published in Chaos Solitons and Fractals (2015).
- [78] C. Tsallis, L. R. da Silva, R. S. Mendes, R. O. Vallejos and A. M. Mariz, Phys. Rev. E **56**, R4922 (1997); L. R. da Silva, R. O. Vallejos, C. Tsallis, R. S. Mendes and S. Roux, Phys. Rev. E **64**, 011104 (2001).
- [79] D. Sornette, Phys. Rep. **297**, 239 (1998).
- [80] M. Rybczyński, G. Wilk and Z. Włodarczyk, EPJ Web of Conf. **90**, 01002 (2015), arXiv:1412.0474.